universe

MDPI

Article

The Sharma–Mittal Model's Implications on FRW Universe in Chern–Simons Gravity

Sarfraz Ali [1], Muhammad Hummad Waheed [2], Muhammad Imran Asjad [3], Khuram Ali Khan [4], Thanin Sitthiwirattham [5,*] and Chanon Promsakon [6]

1 Department of Mathematics, University of Education, Lahore 54700, Pakistan; sarfaraz.ali@ue.edu.pk
2 Riphah International University Faisalabad Campus, Faisalabad 38000, Pakistan; muhammadhammadwaheed@gmail.com
3 Department of Mathematics, University of Management and Technology Lahore, Lahore 54770, Pakistan; imran.asjad@umt.edu.pk
4 Department of Mathematics, University of Sargodha, Sargodha 38000, Pakistan; khuram.ali@uos.edu.pk
5 Mathematics Department, Faculty of Science and Technology, Suan Dusit University, Bangkok 10300, Thailand
6 Department of Mathematics, Faculty of Applied Science, King Mongkut's University of Technology North Bangkok, Bangkok 10800, Thailand; chanon.p@sci.kmutnb.ac.th
* Correspondence: thanin_sit@dusit.ac.th

Abstract: The Sharma–Mittal holographic dark energy model is investigated in this paper using the Chern–Simons modified gravity theory. We investigate several cosmic parameters, including the deceleration, equation of state, square of sound speed, and energy density. According to the deceleration parameter, the universe is in an decelerating and expanding phase known as de Sitter expansion. The Sharma–Mittal HDE model supports a deceleration to acceleration transition that is compatible with the observational data. The EoS depicts the universe's dominance era through a number of components, such as $\omega = 0$, $\frac{1}{3}$, 1, which indicate that the universe is influenced by dust, radiation, and stiff fluid, while $-1 < \omega < \frac{1}{3}$, $\omega = -1$, and $\omega < -1$ are conditions for quintessence DE, ΛCDM, and Phantom era dominance. Our findings indicate that the universe is in an accelerated expansion phase, and this is similar to the observational data.

Keywords: Sharma–Mittal HDE model; FRW universe; Chern–Simons modified gravity

Citation: Ali, S.; Waheed, M.H.; Asjad, M.I.; Khan, K.A.; Sitthiwirattham, T.; Promsakon, C. The Sharma–Mittal Model's Implications on FRW Universe in Chern–Simons Gravity. *Universe* **2021**, 7, 428. https://doi.org/10.3390/universe7110428

Academic Editor: Lorenzo Iorio

Received: 18 October 2021
Accepted: 7 November 2021
Published: 10 November 2021

1. Introduction

An intriguing and longstanding problem that became a genuine test for gravity theories emerged from the observed accelerated expansion of universe [1–3]. The astrophysical findings have given an interesting result that approximately 95–96% of the contents of the cosmos comprise dark matter (DM) and dark energy (DE), along with 4–5% Bayronic matter [4,5]. More intriguingly, about 70% of the energy density is designated as "Dark Energy" and accepted as accountable for the accelerated expansion of the universe [6]. The present astronomical and cosmological models are dealing with these fundamental issues separately. Both DE and DM might be truly quantum gravitational effects or simply a modification of General Relativity (GR) at large distances.

One of the most interesting models in modified theories of gravity in the last couple of decades has been the four-dimensional Chern–Simons modified gravity (CSMG) theory introduced by Jackiw and Pi [7]. The Pontryagin density is the basis of this theory and suggests a violation of parity in Einstein–Hilbert actions. In four-dimensional spacetimes, the density of the Pontryagin term acts as a topological quantity, unless the scalar field Θ is not considered as a coupling constant.

Alexander and Nicolas [8] explored vacuum approximation and exact solutions in CSMG theory and discussed Cosmic Baryon asymmetry and inflation. The energy density

of the universe was explored by Silva and Santos [9] in accordance with Ricci scalar curvature proportionality. Cardoso and Gualtieri [10] studied the stability characteristics and the formalism perturbation of black holes and found no effect on the polar sector of the CS parameter; however, the axial perturbations were found to be associated with a CS scalar field.

The 4-D space times were reassembled in a cotton and Einstein tensor with source-free CSMG theory, and this also demonstrated how the cosmological constant disappears and the null orthogonal hyper-surface Killing vectors became parallel to the CS scalar field [11]. Amarilla et al. [12] suggested an approach that could integrate the null geodesic equation, and this approach explains the black hole's cast shadow. They also discussed that, in addition to the angular momentum of the solution, the CS term distorts the shape of the black hole (BH) shadow.

The geodesic precession and the strong gravitational lensing were addressed by Chen and Jing [13] for slow rotation BH in the dynamical CSMG framework. Gödel type solutions have been explored using a prior prescribed choice of external field as a function of the angular parameter θ, and non-static spherical symmetric metrics were examined as a function of the radial parameter r in [14]. The compatibility of the Gödel metric was examined by Furtado et al. [15] in the context of CSMG. Amir and Ali [16,17] studied different holographic dark energy models in CSMG taking into account the FRW universe. The stability of the Schwarzschild BH in $f(R)$ gravity in the presence of a parity-violating CS term paired with a dynamic scalar field was examined by Moon and Myung [18]. They talked about how $f(R)$ gravity has no effect on the Zerilli equation, while CS coupling has an effect on the Regge–Wheeler equations.

Heavenly in-spirals are one of the best-suited sources of gravity waves for space-based detectors, such as the Laser Interferometer Space Antenna. In particular, GR modifications described in four-dimensional CS gravitational theory are a parameter estimation of EMRIs performed in [19]. Yagi and fellows [20] explored binary and isolated neutron stars in the context of dynamical CSMG theory. They also investigated post-Kepler parameter corrections that were found to be very similar to the double binary pulsar data observed today. The Einstein field equations were solved by Contreras in 2 + 1 dimensional string theory using the minimum geometric deformation method to explore an-isotropic solution [21]. He also evaluated a standard non-regular BH solution that contains exotic or non-exotic hair solutions depending on the cosmological constant.

A variety of entropies have been used to generate modified HDE models [22,23]; however, there is no single example of generalized entropy formalism to construct on the holographic principle available in the literature. The generalized entropies of Rényi [24] and Tsallis [25] are appropriate models for the accelerated universe. These are commonly used to examine different gravitational and cosmological arrangements. Jahromi et al. [26] studied the Sharma–Mittal holographic dark energy model (SMHDE), with the Hubble horizon playing an IR cut-off role, and found that the components of the cosmos did not have any mutual interactions with each other.

The SMHDE model was found to exhibit stable behavior in the case of non-interacting universes [27]. Chen [28] introduced recent developments on holographic entanglement entropy. Varying from regular HDE models with Bekenstein entropy, such models evolve to a late-time accelerated universe. Sharma and Dubey [29] explored the SMHDE models with different diagnostic tools. Nojiri with fellows [30] studied Sharma–Mittal entropic DE and showed that it is indeed equivalent with the generalized HDE.

Dubey et al. [31] explored the accelerated expansion of a conharmonically flat space in relation to an isotropic and spatially homogeneous FRW universe through the SMHDE model. Recently, Younus et al. [32] studied Tsallis, Rényi, and Sharma–Mittal entropies and found a quintessence-like nature of the universe in most of the cases. Sarfraz et al. [33,34] studied the Rényi HDE model considering FRW and Amended FRW matrices in the context of CSMG theory and found a transition from the deceleration to acceleration phase that was fully consistent with the observational data.

Keeping in mind the above motivations, the SMHDE model is used in this paper to investigate the deceleration parameter, energy density, Equation of state (EoS), and square of sound speed in CSMG. These are arranged in the following order. Section 2 discusses the fundamental formulae of CSMG. Section 3 provides a brief overview of the SMHDE model. This section also investigates the deceleration, energy density, and EoS parameters. The final section contains a summary and our concluding remarks.

2. Chern–Simons Modified Gravity

The cancellation of anomalies in particle physics motivates CSMG theory, which is an efficient extension of GR that captures first-order gravitational parity violations. The CS theory is an intriguing deformation of GR that has Pontryagin density as a gravitational parity-violating term in the standard Einstein–Hilbert action as given by

$$S = \int d^4x\sqrt{-g}[\kappa R + \frac{\alpha}{4}\Theta\, {}^*RR - \frac{\beta}{2}(g^{\mu\nu}\nabla_\mu\Theta\nabla_\nu\Theta + 2V[\Theta])] + S_{mat}, \tag{1}$$

where α & β are dimensionless parameters, $\kappa = \frac{1}{16\pi G}$, g is the determinant of the metric, ∇_μ is the covariant derivative, and integrals represent the volume executed anywhere on the manifold v. The term ${}^*RR$ is the Pontryagin density, defined as ${}^*RR = {}^*R^a{}_b{}^{cd}R^b{}_{acd}$, formally, ${}^*RR \propto R \wedge R$, where R is the Ricci scalar curvature. The natural choice for the potential $V[\Theta]$ of the CS coupling is the Cotton tensor. S_{mat} represents some matter Lagrangian density, and Θ is a pseudo-scalar field depending on the space-time coordinates. If it is assumed to be a constant function, then the CSMG theory reduces to GR identically. Taking the action of variation over g and the scalar field Θ in Equation (1), one obtains a set of CSMG equations expressed as

$$G_{pq} + \frac{\alpha}{\kappa}C_{pq} = \frac{1}{2\kappa}T_{pq}, \tag{2}$$

$$g^{pq}\nabla_p\nabla_q\Theta = -\frac{\alpha}{4\pi}{}^*RR \tag{3}$$

where G_{pq}, C_{pq}, and T_{pq} are the Einstein, Cotton, and energy-momentum tensors, respectively. T_{pq} is a combination of the $T^{(m)}_{pq}$ and T^{Θ}_{pq} matter and scalar field components defined as

$$T^{(m)}_{pq} = (p+\rho)U_pU_q - pg_{pq}, \tag{4}$$

$$T^{\Theta}_{pq} = \beta(\partial_p\Theta)(\partial_q\Theta) - \frac{\beta}{2}g_{pq}(\partial^v\Theta)(\partial_v\Theta), \tag{5}$$

The quantity C-tensor is defined mathematically as

$$C^{pq} = -\frac{1}{2\sqrt{-g}}[v_\sigma\epsilon^{\sigma p\gamma\alpha}\nabla_\gamma R^q_\alpha + \frac{1}{2}v_{\sigma\tau}\epsilon^{\sigma q\gamma\alpha}R^{\tau p}_{\gamma\alpha}] + (p \longleftrightarrow q), \tag{6}$$

where $v_\sigma = \nabla_\sigma\Theta$, $v_{\sigma\tau} = \nabla_\sigma\nabla_\tau\Theta$, and ϵ^{cdef} represents the four dimensional Levi–Civita tensor.

The CSMG theory is founded on two explicitly distinct formulations, such as non-dynamical and dynamical formulations. The CS scalar is the aforementioned function in the non-dynamical case, and therefore its nominal transformation consequence enhances to a differential constriction on the space of acceptable systems. In the particular instance of a dynamical composition, the CS term is viewed as a dynamical field, including an effective stress–energy tensor and an evolution equation. The dynamical approach is defined mathematically by allowing α and β to be arbitrary, but non-zero constants in Equation (1) at the level of action. On the other hand, for the non-dynamical framework $\beta = 0$, and α is an arbitrary value at the level of action, such that the scalar field is externally prescribed rather than emerging dynamically.

The curvature of spacetime through which light travels on its path to a planet's surface influences the appearance of structures at cosmic distances. The geometrical attributes of the cosmos are completely described by Einstein's theory of relativity in which the metric is a fundamental quantity that describes the geometry of spacetime. In a homogeneous and isotropic universe, the curvature of space may vary with time; however, its magnitude remains unchanged at any given epoch since the Big Bang. Robertson and his colleagues independently demonstrated in the mid-1930s that the FRW metric would be the most generic form for representing the expansion of the universe, mathematically described as

$$ds^2 = dt^2 - a^2(t)[\frac{1}{1-kr^2}dr^2 + r^2(d\theta^2 + \sin^2\theta d\phi^2)]. \tag{7}$$

Using Equation (5) the 00-component of the energy momentum tensor is calculated as

$$T_{00}^{\Theta} = \frac{1}{2}\dot{\Theta}^2. \tag{8}$$

For the FRW metric, the Pontryagin term ${}^*RR$ turned to be zero identically, and thus the second CS field equation given in Equation (3), reduces to

$$g^{pq}\nabla_p\nabla_q\Theta \quad = g^{pq}\left[\partial_p\partial_q\Theta - \Gamma^o_{pq}\partial_o\Theta\right] = 0 \tag{9}$$

The analytic solution of the above equation is

$$\dot{\Theta} \quad = ca^{-3} \tag{10}$$

Substituting Equation (10) in Equation (8)

$$\rho_\theta = T_{00}^{\theta} = \rho_{\theta_0}a^{-6}, \tag{11}$$

where $\rho_{\theta_0} = \frac{1}{2}m^2$, and m is the integration constant.

3. Sharma–Mittal HDE Model

Significantly increasing and additive properties are not always preserved in systems involving statistical mechanics and associated thermodynamics at large distances. Shannon's entropy [35] serves to create interactions that have a smooth and convoluted function based on all possibilities, such as the P_j criterion of the $\sum_{j=1}^{W} P_j = 1$ system with jth probability of P_j. These are generally better described systems, i.e., $P_i^{1-\sigma}$, which are more inclined to be σ, instead of the usual transmission of P_j, by the distribution of the probabilities. It is consequently necessary to describe these systems through other entropy measures. Sharma and Mittal [36,37] proposed a general entropy, such as

$$S_{SM} = \frac{1}{1-\gamma}\left[\left(\sum_{j=1}^{W} P_j^{1-\sigma}\right)^{\frac{1-\gamma}{\sigma}} - 1\right]. \tag{12}$$

In the case of BH entropy in a loop, quantum gravity $\sum_{j=1}^{W} P_j^{1-\sigma} = 1 + \frac{\sigma A}{4}$ in Equation (12)

$$S_{SM} = \frac{1}{\zeta}\left[\left(1 + \frac{\sigma A}{4}\right)^{\frac{\zeta}{\sigma}} - 1\right], \tag{13}$$

where A is the horizon area, $\zeta = 1 - \gamma$, and γ is a free parameter. On the basis of the holographic principle, a relation $\Lambda^4 \propto \frac{S}{L^4}$ is constructed for L, Λ, and S, which are the IR , UV cut-off, and system horizon, respectively. According to the HDE hypothesis, the DE

density ρ_d corresponding to the IR cut-off in the presence of $H = L^{-1} = \sqrt{\frac{4\pi}{A}}$ is expressed as

$$\rho_d = \frac{3\lambda^2 H^4}{8\pi\zeta}\left[\left(1+\frac{\sigma\pi}{H^2}\right)^{\frac{\zeta}{\sigma}}-1\right], \tag{14}$$

The term $\frac{3\lambda^2}{8\pi}$ stands for a proportionality constant, and λ stands for a free dimensionless parameter. The original HDE model can also be derived choosing the appropriate limit of $\zeta \to \sigma$.

Since all the components of the Cotton tensor turned to be zero identically, the first Friedmann equation of CSMG theory for flat universe takes the form

$$H^2 = \frac{8\pi}{3}(\rho_m + \rho_d + \rho_\theta), \tag{15}$$

$\rho_m = \rho_o a^{-3}$ represents the matter energy density. Inserting the expression for ρ_m, ρ_d, and ρ_θ in Equation (15), it looks like

$$H^2 = \frac{8\pi}{3}\left(\rho_o a^{-3} + \rho_{\theta_0} a^{-6} + \frac{3\lambda^2 H^4}{8\pi\zeta}\left[\left(1+\frac{\sigma\pi}{H^2}\right)^{\frac{\zeta}{\sigma}}-1\right]\right). \tag{16}$$

For the sake of simplicity, we assume that $H = \Phi(z)H_o$, where H_o stands for the initial value of the Hubble parameter and in terms of the redshift parameter, the scale factor is $a(t) = [z+1]^{-1}$. Introducing $\Omega_m = \frac{8\pi}{3H_o^2}\rho_o$, $\Omega_\theta = \frac{8\pi}{3H_o^2}\rho_{\theta_0}$ and $\chi = \frac{\zeta}{\sigma}$, Equation (16) becomes

$$\begin{aligned}\Phi^2(z) &= \Omega_\theta[z+1]^6 + \Omega_m[z+1]^3 + \frac{\lambda^2\Phi^4(z)}{\zeta} \\ &\quad \times\left[\left(1+\frac{\sigma\pi}{\Phi^2(z)H_o^2}\right)^{\chi}-1\right].\end{aligned} \tag{17}$$

The factor $\frac{\lambda^2}{\zeta}$ is constant to be solved at $z = 0$ and $\Phi(0) = 1$, such that

$$\frac{\lambda^2}{\zeta} = \frac{1-\Omega_m-\Omega_\theta}{\left(1+\frac{\sigma\pi}{H_o^2}\right)^{\chi}-1}. \tag{18}$$

Substituting Equation (18) in Equation (17), it becomes

$$\begin{aligned}\Phi^2(z) &= \Omega_\theta[z+1]^6 + \Omega_m[z+1]^3 \\ &+ \frac{1-\Omega_m-\Omega_\theta}{\left(1+\frac{\sigma\pi}{H_o^2}\right)^{\chi}-1}\Phi^4(z)\left[\left(1+\frac{\sigma\pi}{\Phi^2(z)H_o^2}\right)^{\chi}-1\right].\end{aligned} \tag{19}$$

The deceleration parameter q is a dimension-free parameter used to investigate the expansion rate of the universe affected by self-gravity. The relation between q and H is given mathematically as

$$q = -1 - \frac{\dot{H}}{H^2}. \tag{20}$$

We assume that $H(z) = H_o\Phi(z)$ and substitute $\dot{H} = H_o\frac{d}{dz}(\Phi(z))$ into Equation (20) to obtain

$$q = -(1 + \frac{H_o\frac{d}{dz}(\Phi(z))}{H_o^2\Phi^2(z)}). \tag{21}$$

Hence, the deceleration parameter in terms of z is

$$q = -1 + H_o^4[z+1]^7 \times \left[\frac{3\Omega_m + 6\Omega_\theta[z+1]^3}{2H_o^2[z+1]^2 - 4(\frac{1-\Omega_m-\Omega_\theta}{\left(1+\frac{\sigma\pi}{H_o^2}\right)^\chi - 1})[\{(1+\sigma\pi[z+1]^2)^\chi - 1\} + 2\chi\sigma\pi[z+1]^2(1+\sigma\pi[z+1]^2)^{\chi-1}]} \right]. \quad (22)$$

To analyze the behavior of q, we give a graphical representation using different numerical values of the parameters employed in Equation (22), such that $\Omega_\theta = 0.15, 0.17, 0.19$, $H_o = 67.4$, $\Omega_m = 0.315$, $\sigma = -25$ and $\chi = 5$, corresponding to the blue, red, and green lines, respectively. Figure 1 illustrates the decelerated phase $q < 0$ at $z < 0$ and takes a flip over the accelerated phase for $q > 0$ at a high redshift. The behavior of the deceleration parameter is observed to be fairly analogous, and our graph supports the shift from deceleration to acceleration, as anticipated in [2,4,17,32,38,39]. It is worth mentioning here that the SMHDE model supports the deceleration to acceleration conversion well-matched with the observational data.

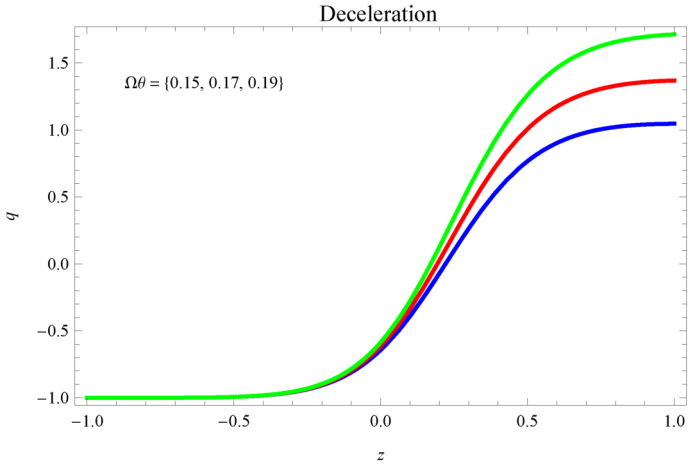

Figure 1. q versus z.

The total density Ω_0 of the universe is defined as

$$\Omega_0 = \frac{\rho}{\rho_c}. \quad (23)$$

If $\Omega_0 = 1$, this represents a flat universe, and there is adequate matter to prevent it from expanding but not enough to cause it to collapse. Regular baryonic matter (Ω_B), DM (Ω_D), and DE (Ω_Λ) are the three components of the density parameter. The DM density parameter $\rho_d = \Omega_D(z)\frac{3H_o^2}{8\pi}$ was used in Equation (14) to arrive at

$$\Omega_D(z)\frac{3H_o^2}{8\pi} = \frac{3\lambda^2 H_o^4}{8\pi\zeta}\left[\left(1+\frac{\sigma\pi}{H^2}\right)^\chi - 1\right]. \quad (24)$$

In terms of the redshift parameter, it can be written as

$$\Omega_D(z) = \frac{\lambda^2}{H_o^2[z+1]^4\zeta}\left[(1+\sigma\pi[z+1])^\chi - 1\right]. \quad (25)$$

To analyze the stability of the Sharma–Mittal model, we adopted the technique of a square of sound speed (v_s^2) given by

$$v_s^2 = \frac{dp_d}{d\rho_d} = \frac{\frac{dp_d}{d\Phi(z)}}{\frac{d\rho_d}{d\Phi(z)}}. \tag{26}$$

Consider a scenario in which there is no interaction between various components of the universe, implying that the SMHDE model follows the ordinary conservation law.

$$p_d = -\left(\frac{\dot{\rho_d}}{3H} + \rho_d\right) = -\left(\frac{\rho_d' \dot{H}}{3H} + \rho_d\right), \tag{27}$$

where $\rho_d' = \frac{d\rho_d}{dH}$, and dot denotes the derivative with respect to time. The second field equation for the flat FRW metric is

$$H^2 + \frac{2}{3}\dot{H} = \frac{-8\pi}{3} p_d. \tag{28}$$

Substituting Equation (27) in (28) analytically, one obtains

$$p_d = \frac{\rho_d - \frac{\Phi(z)}{2}\frac{d\rho_d}{d\Phi(z)}}{\left(\frac{4\pi}{3H_o^2\Phi(z)}\right)\frac{d\rho_d}{d\Phi(z)} - 1}. \tag{29}$$

By differentiation of Equations (14) and (29) w.r.t $\Phi(z)$ and substituting the corresponding expressions in Equation (26), one arrives at

$$\begin{aligned}
v_s^2 &= -\frac{H_0^3[z+1]^2}{24\pi\Big(-[z+1]^2\pi K\chi\sigma(1+\pi\sigma[z+1]^2)^{\chi-1} + 2(-1+(1+\pi\sigma[z+1]^2)^{\chi})\Big)} \\
&\times \frac{1}{\left(-H_0^3[z+1]^3 + -2 - \pi[z+1]^2 K\chi\sigma(1+\pi[z+1]^2\chi)^{\chi-1} + 2(1+\pi[z+1]^2\chi)\right)^2} \\
&\times \{12\pi[z+1]\{H_o^2[z+1]^2 + \pi[z+1]^2 K\chi\sigma(1+\pi[z+1]^2\chi)^{\chi-1} \\
&- 2(-1(1+\pi[z+1]^2\chi))^{\chi}\}\{-H_0^3\pi^2[z+1]^5 K(\chi-1)\chi\sigma^2(1+\pi\sigma[z+1]^2)^{\chi-2} \\
&+ 5H_o(-1+H_o^2)\pi[z+1]^3 K\chi\sigma(1+\pi\sigma[z+1]^2)^{\chi-1} \\
&- 6K(-1+(1+\pi\sigma[z+1]^2)^{\chi}) - H_o[z+1]\{\pi[z+1]^2 K\chi\sigma(1+\pi\sigma[z+1]^2)^{\chi-1} \\
&- 2(-1+(1+\pi\sigma[z+1]^2)^{\chi})\}\} + \{3H_o\pi[z+1]^2 K\chi\sigma(1+\pi\sigma[z+1]^2)^{\chi-1} \\
&- 6H_o(-1+(1+\pi\sigma[z+1]^2)^{\chi}) - 4\pi[z+1]K\{-2H_0^3\pi^2[z+1]^3(\chi-1)\chi\sigma^2 \\
&\times (1+\pi\sigma[z+1]^2)^{\chi-2} + 5H_o(H_o^2-1)\pi[z+1]^3\chi\sigma(1+\pi\sigma[z+1]^2)^{\chi-1} \\
&- 6(-1+(1+\pi\sigma[z+1]^2)^{\chi})\}\}\{3\pi[z+1]^2 K\chi\sigma(1+\pi\sigma[z+1]^2)^{\chi-1} \\
&- 6(-1+(1+\pi\sigma[z+1]^2)^{\chi}) + 8H_o^2\pi[z+1]^4\rho_d\}\}.
\end{aligned} \tag{30}$$

For the sake of simplicity, we assume $\left(\frac{1-\Omega_m-\Omega_\theta}{\left(1+\frac{\sigma\pi}{H_o^2}\right)^{\chi}-1}\right) = K$ in Equation (30). Now, we plot a graph of v_s^2 versus the red shift parameter.

In Figure 2, we produced a graph of v_s^2 vs z with the values $H_o = 67.4$, $\Omega_m = 0.315$, $\sigma = 20$, $\rho = 0.8$, $\chi = -10, -20, -40$, and $\Omega_\theta = 0.15, 0.17, 0.19$, corresponding to the blue, red, and green lines, respectively. It is definitely a positive function that shows a decreasing tendency for some $-1 < z < -0.6$ for the future but remains positive today.

The expression of EoS for an ideal fluid is given by

$$\omega = \frac{p_d}{\rho_m + \rho_d + \rho_\theta}. \tag{31}$$

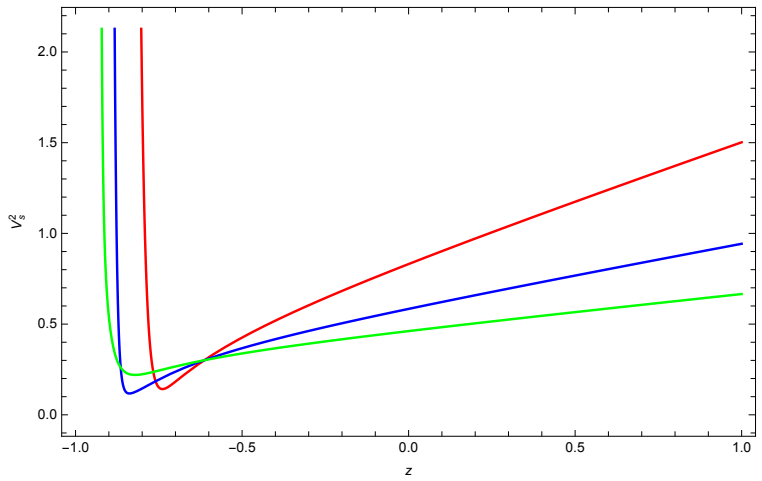

Figure 2. v_s^2 versus z.

The EoS is a mathematical model that is used to investigate the effects of various quantities on the cosmos. For example $\omega = 0$ represents that the universe is influenced by relativistic matter. The radiation era has an effect on the decelerated phase of the universe if $0 < \omega < \frac{1}{3}$. The phantom, cosmological constant, and quintessence erases are found at $\omega < -1$, $\omega = -1$, and $\omega < -\frac{1}{3}$, respectively.

The expression for the EoS is evaluated as

$$\begin{aligned} \omega &= -1 + \frac{2}{3} H_o^4 [z+1]^7 \\ &\times \left[\frac{3\Omega_m + 6\Omega_\theta [z+1]^3}{2H_o^2 [z+1]^2 - 4K[\{(1+\sigma\pi[z+1]^2)\chi - 1\} + 2\chi\sigma\pi[z+1]^2(1+\sigma\pi[z+1]^2)\chi^{-1}]} \right]. \end{aligned} \tag{32}$$

To analyze the behavior of the EoS parameter with respect to the redshift, a graph is plotted.

In Figure 3, a graph is plotted for ω versus z taking into account the parametric values of $H_o = 67.4$, $\Omega_m = 0.315$, $\sigma = 3$, $\chi = 16$, and $\Omega_\theta = 0.15, 0.17, 0.19$, corresponding to blue, red, and green, respectively. The graphical representation reveals that the universe is influenced by DE, as EoS anticipates the accelerated expansion phase [16,17,22,26–28,32].

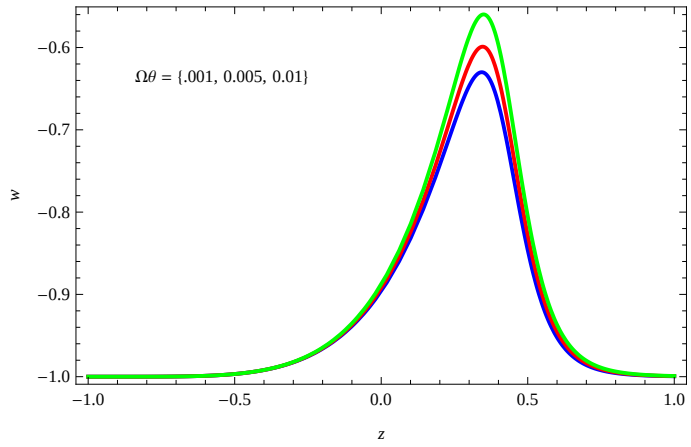

Figure 3. ω versus z.

In the absence of χ or σ, the EoS is given as

$$\omega = -1 + 3H_o^4 \left[3[z+1]\Omega_m + \frac{6\Omega_\theta}{[z+1]^4} \right]. \tag{33}$$

The $\omega - \omega'$ plane is used to investigate the universe's dynamical features. It has two zones: one for thawing and one for freezing. The EoS parameter (ω) was negative in the thawing zone and turned positive in the evolutionary case; however, the value of the EoS parameter (ω) stayed negative in the freezing region.

The term ω' is a derivative of EoS with respect to z of (32), and simplification gives

$$\begin{aligned}\omega' = & \frac{1}{\{2H_o^2[z+1]^2+2\pi K\chi\sigma(1+\pi\sigma[z+1]^2)^{\chi-1}-4K(-1+(1+\pi\sigma[z+1]^2)^{\chi})\}^2} \\ \times & \{12H_o^2[z+1]^6\{5H_o^2[z+1]^2\Omega_m - 2\pi^2K\chi\sigma^2\Omega_m(\chi-1)[z+1]^4(1+\pi\sigma[z+1]^2)^{\chi-2} \\ + & 9\pi K\chi\sigma[z+1]^2(1+\pi\sigma[z+1]^2)^{\chi-1} - 14K\Omega(-1+(1+\pi\sigma[z+1]^2)^{\chi}) \\ + & 24\pi K\sigma\Omega_\theta[z+1]^5(1+\pi\sigma[z+1]^2)^{\chi-1} - 40K\Omega_\theta[z+1]^3(-1+(1+\pi\sigma[z+1]^2)^{\chi}) \\ + & 16H_o^2\Omega_\theta[z+1]^5 - 4\pi^2K\sigma^2\chi(\chi-1)\Omega_\theta[z+1]^7(1+\pi\sigma[z+1]^2)^{\chi-2}\}\}. \end{aligned} \quad (34)$$

In Figure 4, the graph is plotted for ω' vs z at $H_o = 67.4$, $\Omega_m = 0.315$, $\sigma = -40$, $\chi = 3$, and $\Omega_\theta = 0.15, 0.17, 0.19$ corresponding to blue, red, and green, respectively. The term ω' shows negative behavior depending on the choice of $\chi > 0$ and $\sigma > 0$.

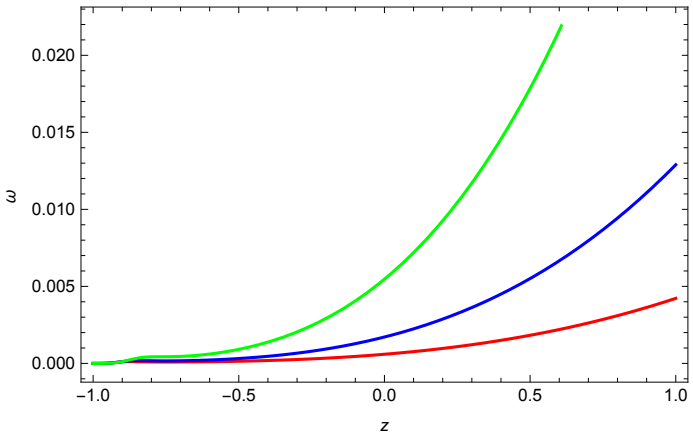

Figure 4. ω' and z.

4. Discussion of the Results and Conclusions

The SMHDE model was studied in this manuscript within the framework of CSMG theory while taking into account the FRW universe. We studied the deceleration parameter, EoS, the square of sound speed, and the energy density as cosmological parameters. We predicted that the universe is in a decelerating and expanding phase known as de Sitter expansion. At a high redshift, the graphical behavior depicted the decelerated phase $q < 0$ and flipped over the accelerated phase for $q > 0$.

We concluded that deceleration parameter was identical in all three cases, and we propose that the conversion from deceleration to acceleration is coherent with those of [2,4,7,17,22,32,38,39]. It is important to note that the SMHDE model endorses a deceleration to acceleration transition that is congruent with the observational data. Various values of EoS, for example $\omega = 0, \frac{1}{3}, 1$, indicate that the universe is influenced by dust, radiation, and stiff fluid, while ($\omega = -\frac{1}{3}$ and -1 and $\omega < -1$) stand for quintessence, ΛCDM, and Phantom erases, respectively. Our findings demonstrated that the universe is being influenced by DE as the EoS anticipated accelerated expansion phases similar to those of [16,17,22].

The density parameter of the SMHDE model is well defined for all values of χ and $\sigma > 0$. It is clear that the density parameter showed decreasing behavior and asymptotically converged to zero, implying that the cosmos approaches a De Sitter universe with eternally accelerated expansion. The square speed of sound was positive for all parameter values that predict system stability. The dynamical properties of the universe were studied using the ω' in terms of the thawing and freezing regions. The EoS parameter ω turned negative

in the thawing region and positive in the evolutionary case, whereas the significance of the EoS parameter remained negative in the freezing region.

Author Contributions: All the authors contributed equally. All authors have read and agreed to the published version of the manuscript.

Funding: This research was funded by King Mongkut's University of Technology North Bangkok. Contract no.KMUTNB-64-KNOW-48.

Institutional Review Board Statement: Not applicable.

Informed Consent Statement: Not applicable.

Data Availability Statement: Not applicable.

Acknowledgments: The authors are greatly obliged and thankful to the University of Management and Technology Lahore, Pakistan for facilitating and supporting this research work.

Conflicts of Interest: The authors declare no conflict of interest.

References

1. Riess, A.G.; Filippenko, A.V.; Challis, P.; Clocchiatti, A.; Diercks, A.; Garnavich, P.M.; Gilliland, R.L.; Hogan, C.J.; Jha, S.; Kirshner, R.P. Observational Evidence from Supernovae for an Accelerating Universe and a Cosmological Constant. *Astron. J.* **1998**, *116*, 1009–1038. [CrossRef]
2. Perlmutter, S.; Aldering, G.; Goldhaber, G.; Knop, R.A.; Nugent, P.; Castro, P.G.; Deustua, S.; Fabbro, S.; Goobar, A.; Groom, D.E.; et al. Measurements of Ω and ∧ from 42 High-Redshift Supernovae. *Astrophys. J.* **1999**, *517*, 565–586. [CrossRef]
3. Tonry, J.L.; Schmidt, B.P.; Barris, B.; Candia, P.; Challis, P.; Clocchiatti, A.; Coil, A.L.; Filippenko, A.V.; Garnavich, P.; Hogan, C.; et al. Cosmological Results from High-z Supernovae. *Astrophys. J.* **2003**, *594*, 1–24. [CrossRef]
4. Bernardis, P.d.; Ade, P.A.R.; Bock, J.J.; Bond, J.R.; Borrill, J.; Boscaleri, A.; Coble, K.; Crill, B.P.; Gasperis, G.D.; Farese, P.C.; et al. A Flat Universe from High-Resolution Maps of the Cosmic Microwave Background Radiation. *Nature* **2000**, *404*, 955–959. [CrossRef] [PubMed]
5. Hanany, S.; Ade, P.; Balbi, A.; Bock, J.; Borrill, J.; Boscaleri, A.; de Bernardis, P.; Ferreira, P.G.; Hristov, V.V.; Jaffe, A.H.; et al. MAXIMA-1: A Measurement of the Cosmic Microwave Background Anisotropy on angular scales of 10 arcminutes to 5 degrees. *Astrophys. J.* **2000**, *545*, L5. [CrossRef]
6. Peebles, P.J.E.; Ratra, B. The Cosmological Constant and Dark Energy. *Phys. Rev. D* **2003**, *75*, 559–606. [CrossRef]
7. Jackiw, R.; Pi, S.Y. Chern Simons Modification of General Relativity. *Phys. Rev. D* **2003**, *68*, 10. [CrossRef]
8. Alexander, S.; Nicolas, Y. Chern–Simons Modified General Relativity. *Phys. Rep.* **2009**, *480*, 1–55. [CrossRef]
9. Silva, J.G.; Santos, A.F. Ricci dark energy in Chern–Simons modified gravity. *Eur. Phys. J. C* **2013**, *73*, 2500. [CrossRef]
10. Cardoso, V.; Gualtieri, L. Perturbations of Schwarzschild black holes in dynamical Chern–Simons modified gravity. *Phys. Rev. D* **2009**, *80*, 6. [CrossRef]
11. Ahmedov, H.; Aliev, A.N. Decoupling and Reduction in Chern–Simons Modified Gravity. *Phys. Lett. B* **2010**, *690*, 196–200. [CrossRef]
12. Amarilla, L.; Eiroa, E.F.; Giribet, G. Null geodesics and shadow of a rotating black hole in extended Chern–Simons modified gravity. *Phys. Rev. D* **2010**, *81*, 12. [CrossRef]
13. Chen, S.; Jing, J. Geodetic precession and strong gravitational lensing in dynamical Chern–Simons-modified gravity. *Class Quantum Gravity* **2010**, *27*, 22. [CrossRef]
14. Ali, S.; Amir, M.J. A study of important solutions in Chern–Simons modified gravity. *Indian J. Phys.* **2019**, *94*, 1837–1845. [CrossRef]
15. Furtado C.; Pi, S.Y. The Godel metric in the Chern–Simons modified gravity. *Int. J. Mod. Phys. B Conf. Ser.* **2012**, *18*, 145–149. [CrossRef]
16. Amir, M. J.; Ali, S., Ricci Dark Energy of Amended FRW Universe in Chern-Simon Modified Gravity. *Int. J. Theor. Phys.* **2015**, *54*, 1362–1369. [CrossRef]
17. Amir, M.J.; Ali, S. A Study of Holographic Dark Energy Models in Chern-Simon Modified Gravity. *Int. J. Theor. Phys.* **2016**, *55*, 50–95.
18. Myung, Y.S.; Moon, T.; Son, E.J. Stability of f(R) black holes. *Phys. Rev. D* **2011**, *84*, 12.
19. Canizares, P.; Gair, J.R.; Sopuerta, C.F. Testing Chern–Simons modified gravity with observations of extreme-mass-ratio binaries. *J. Phys. Conf. Ser.* **2012**, *363*, 012019. [CrossRef]
20. Yagi, K.; Stein, L.C.; Yunes, N.; Tanaka, T. Isolated and binary neutron stars in dynamical Chern–Simons gravity. *Phys. Rev. D* **2013**, *87*, 8. [CrossRef]
21. Contreras, E. Gravitational decoupling in 2+1 dimensional space–times with cosmological term. *Class Quantum Gravity* **2019**, *36*, 9. [CrossRef]
22. Wang, S.; Wang, Y.; Li, M. Holographic Dark Energy. *Phys. Rep.* **2017**, *696*, 1–57. [CrossRef]

23. Wang, B.; Abdalla, E. ;Barandela, F.; Pavon, D. Dark matter and dark energy interactions: Theoretical challenges, cosmological implications and observational signatures. *Rep. Prog. Phys.* **2016**, *79*, 9. [CrossRef] [PubMed]
24. Rènyi, A. *Probability Theory*; North-Holland: Amsterdam, The Netherlands, 1970.
25. Tsallis, C. The Nonadditive Entropy Sq and Its Applications in Physics and Elsewhere: Some Remarks. *Entropy* **2011**, *13*, 1765–1804. [CrossRef]
26. Jahromi, A.S. Generalized entropy formalism and a new holographic dark energy model. *Phys. Lett. B* **2018**, *780*, 21–24. [CrossRef]
27. Moradpour, H.; Moosavi, S.A.; Lobo, I.P.; Morais, J.P.; Jawad, A.; Salako, I.G. Thermodynamic approach to holographic dark energy and the Rènyi entropy. *Eur. Phys. J. C* **2018**, *78*, 829. [CrossRef]
28. Chen, B. Holographic entanglement entropy: A topical review. *Commun. Theor. Phys.* **2019**, *71*, 837. [CrossRef]
29. Sharma, U.K.; Dubey, V.C. Exploring the Sharma–Mittal HDE models with different diagnostic tools. *Eur. Phys. J. Plus* **2020**, *135*, 391. [CrossRef]
30. Nojiri, S.; Odintsov, S.D.; Paul, T. Fifferent faces of generalized holographic dark energy. *Symmetry* **2021**, *13*, 928. [CrossRef]
31. Dubey, V.C.; Sharma, U.K.; Pradhan, A. Sharma–Mittal holographic dark energy model in conharmonically flat space-time. *Int. J. Geom. Methods Mod. Phys.* **2021**, *18*, 1. [CrossRef]
32. Younas, M.; Jawad, A.; Qummer, S.; Moradpour, H.; Rani, S. Cosmological Implications of the Generalized Entropy Based Holographic Dark Energy Models in Dynamical Chern–Simons Modified Gravity. *Adv. High Energy Phys.* **2019**, *2019*, 1287932. [CrossRef]
33. Sarfraz, A.; Sabir, I.; Khan, A.K.; Hamid, R.M. Amended FRW Metric and Rényi Dark Energy Model. *Adv. High Energy Phys.* **2021**, *2021*, 9704909.
34. Sarfraz, A.; Sarfaraz, K.; Sadia, S.; Amare, A. The Renyi holographic dark energy model in Chern–Simons gravity: Some cosmological implications. *Int. J. Geom. Methods Mod. Phys.* **2021**, *18*. [CrossRef]
35. Shannon, C.E. A Mathematical Theory of Communicatio. *Bell Syst. Tech. J.* **1948**, *27*, 379. [CrossRef]
36. Sharma, B.D.; Mittal, D.P. New non-additive measures of entropy for discrete probability distributions. *J. Math. Sci.* **1975**, *10*, 28–40.
37. Sharma, B.D.; Mittal, D.P. New non-additive measures of relative information. *J. Comb. Inf. Syst. Sci.* **1977**, *2*, 4.
38. Ma, Y.Z. Variable cosmological constant model: The reconstruction equations and constraints from current observational data. *Nucl. Phys. B* **2008**, *804*, 262–285. [CrossRef]
39. Daly, R.A.; Djorgovski, S.G.; Freeman, K.A.; Mory Matthew, P.; O'Dea, C.P.; Kharb, P.; Baum, S. Improved constraints on the acceleration history of the universe and the properties of the dark energy. *Astrophys. J.* **2008**, *677*, 1–11. [CrossRef]